A study of tracer and collective diffusional processes in α'-$NbD_{0.7}$ at 600 K using quasielastic neutron scattering with spin analysis

1990 J. Phys.: Condens. Matter 2 79

(http://iopscience.iop.org/0953-8984/2/1/006)

J. Phys.: Condens. Matter 2 (1990) 79–94. Printed in the UK

A study of tracer and collective diffusional processes in α'-$NbD_{0.7}$ at 600 K using quasielastic neutron scattering with spin analysis

J C Cook†, D Richter†, O Schärpf†, M J Benham‡, D K Ross‡, R Hempelmann§, I S Anderson‖ and S K Sinha¶

† Institut Laue–Langevin, 156X Centre de Tri, 38042 Grenoble, France

‡ School of Physics and Astrophysics, University of Birmingham, Birmingham B15 2TT, UK

§ Institut für Festkörperforschung, Kernforschungsanlage, D-5170 Jülich, Federal Republic of Germany

‖ Paul Scherrer Institut, 5234 Villigen, Switzerland

¶ Exxon Research and Engineering Company, Annandale, New Jersey, USA

Received 26 May 1989, in final form 14 August 1989

Abstract. We have used neutron polarisation analysis to measure, separately, the self and collective dynamics of a high-concentration lattice gas of deuterium in a single crystal of niobium. The measured incoherent scattering has been found to be well described by the dynamical model due to Rowe *et al* and the coherent scattering function is adequately described by a simple adaptation of this model, in which the quasielastic line width narrows with increases in the structure factor, $S(Q)$. Estimates of the diffusion coefficients and correlation factors appropriate to tracer and collective processes, together with the thermodynamic factor, have been determined from model fitting. Information on the interstitial ordering and the extent of the interactions has also been deduced and is in accordance with current Monte-Carlo predictions (Faux and Ross) within the bounds of the expected site blocking and availability. We believe this experiment to be the first to employ the polarisation analysis technique to study tracer and collective diffusion.

1. Introduction

Recent developments in the theory of collective motions of light interstitials in metal lattices (Sinha and Ross 1988) have inspired neutron scattering studies of the collective response of hydrogen (as determined from coherent quasielastic neutron scattering) as well as the self-correlation, which is exhibited in the incoherent scattering. The high-concentration NbD system of the present investigation, in which the interstitial diffusion process takes place over a non-Bravais lattice of sites of tetrahedral symmetry, also provides a possible starting model system for AgI-type superionic conductors. Deuterium is used as the interstitial species, because for deuterium, the coherent thermal neutron scattering cross section, σ_{coh}, is comparable in magnitude with the incoherent scattering cross section, σ_{inc} ($\sigma_{coh} = 5.6$ b, $\sigma_{inc} = 2.0$ b), in contrast with hydrogen where 98% of the total scattering cross section is incoherent.

There are two possible approaches to the problem of separating the incoherent and coherent components of the total scattering. The first was employed by Hempelmann *et*

0953-8984/90/010079 + 15 $03.50

Table 1. Relative neutron–nuclear interaction probabilities for spin flip and non-spin-flip scattering.

		Incoherent	
	Coherent	Spin	Isotope
	I_1	I_2	I_3
↑ ↑	1	1/3	1
↑ ↓	0	2/3	0

al (1988) and involved a theoretical separation of the two parts by model fitting to the total scattering. The second approach, used in the present investigation, is an experimental separation by neutron polarisation analysis. Both techniques have their relative merits and disadvantages. The former requires a significant line broadening difference and good statistics (in order to separate reliably the two components by fitting procedures) and this in turn requires reliable models. The latter, for supermirror polariser and analyser elements, suffers from a rather large attenuation of the cold neutron flux. This is due to the inevitable collimation imposed by these components and the transmission generally decreases as the neutron energy increases for a given beam collimation. A typical value is around 30% (Schärpf 1989b) at the incident energy of the present investigation. Furthermore, the count rate is reduced even further by the fact that only one spin state is measured at any given time and the 'effective transmission' over the course of the experiment is thus nearer 15%. Polarisation analysis also suffers from a more complicated data reduction and multiple-scattering correction, but, however, has the advantage of giving an entirely unambiguous separation of any combination of coherent and incoherent line broadenings. The scattered spin state probabilities can be predicted by quantum mechanics and are summarised in table 1 for the present case of zero nuclear polarisation. From table 1, it can be seen that, for single isotope scattering and in the absence of multiple scattering, the neutrons scattered with spin flip originate entirely from incoherent events and that if one half of this spectrum is subtracted from the non-spin-flip component, we are left with events only from the coherent response. The spin flip scattering is then renormalised by a factor of $\frac{3}{2}$ to obtain the incoherent part in the correct proportion.

2. Theory

A development of the Chudley–Elliott model (Chudley and Elliott 1961) to deal with nearest-neighbour jump diffusion on the tetrahedral symmetry interstitial lattice in a BCC host lattice was proposed by Rowe *et al* (1971). In the tetrahedral symmetry there are six sites per unit cell which are inequivalent with respect to the spatial distribution of nearest-neighbour jump vectors. When calculating the real space probability rate equations for nearest-neighbour jumps, the jump vector is, in general, labelled by three indices; two to label the origin and target site local symmetries (i and j respectively) and one to label sites of a given local symmetry j which are adjacent to the origin site. For the tetrahedral symmetry, however, the third label may be excluded since the four

nearest-neighbour sites always have a different local symmetry. The nearest-neighbour jump process (assuming equal jump rates from each type of site) for the tetrahedral interstitial lattice is then described by six coupled rate equations of the kind

$$\mathrm{d}P(\boldsymbol{r}+\boldsymbol{d}_i, t)/\mathrm{d}t = \frac{1}{4\tau}\sum_j \left(P(\boldsymbol{r}+\boldsymbol{d}_i+\boldsymbol{l}_{ij}, t) - P(\boldsymbol{r}+\boldsymbol{d}_i, t)\right) \qquad i = 1, 6$$

where $\boldsymbol{r}$ is a vector to some fixed origin in an interstitial lattice unit cell, $\boldsymbol{d}_i$ is a vector linking $\boldsymbol{r}$ with site i in the unit cell and $\boldsymbol{l}_{ij}$ is the vector linking site i with an adjacent site j. The sum is over all sites j which are nearest neighbours to site i. The probability of finding an atom at any site i in the unit cell at $\boldsymbol{r}$ for a starting point m (which may be outside the unit cell) and at time t is just the sum of the occupation probabilities at time t for each site in the unit cell given that the particle started at site m:

$$P^m(\boldsymbol{r}, t) = \sum_i P(\boldsymbol{r}+\boldsymbol{d}_i, t).$$

The self-correlation function for the unit cell at $\boldsymbol{r}$, $G_s(\boldsymbol{r}, t)$, is the probability of finding an atom in the unit cell at $\boldsymbol{r}$ at time t given that it was at the origin, m, at $t = 0$, averaged over all the possible starting points, m, of the atom and is therefore given by

$$G_s(\boldsymbol{r}, t) = \frac{1}{6}\sum_m P^m(\boldsymbol{r}, t)$$

subject to the initial conditions:

$$P(\boldsymbol{r}+\boldsymbol{d}_i, 0) = \delta(\boldsymbol{r}) \qquad i = m$$
$$= 0 \qquad i \neq m.$$

The factor $\frac{1}{6}$ in the expression for the self-correlation function implies equal occupation probabilities for each type of site which is only truly valid in the non-interacting case or low-concentration limit. The behaviour in reciprocal space is obtained by solving the rate equations under Fourier transform, which yields a 6×6 matrix eigenvalue problem of the form

$$\mathbf{A}\boldsymbol{I}_j = \lambda_j \boldsymbol{I}_j \tag{1}$$

where $\mathbf{A}$ is the dynamical matrix, $\{\boldsymbol{I}_j\}$ $(j = 1, 6)$ is the set of solution eigenvectors and λ_j are the corresponding eigenvalues. In a general crystal direction, this gives the incoherent scattering function as a sum of six components, which are Lorentzians in energy transfer in the absence of correlations, thus:

$$S_{\mathrm{inc}}(\boldsymbol{Q}, \omega) = \frac{1}{\pi}\sum_{j=1}^{6} \frac{W_j\lambda_j/\tau}{(\lambda_j/\tau)^2 + \omega^2}\,\mathrm{e}^{-2W} \tag{2}$$

where e^{-2W} is the Debye–Waller factor, τ is the charcteristic time between jumps (or residence time) of the interstitial and W_j are the Lorentzian weights. For equal site energies in the tetrahedral system, these are given by

$$W_k = \frac{1}{6}\sum_i \sum_j (\alpha_i^k)^* \alpha_j^k \tag{3}$$

where α_i^k is the ith component of the kth solution vector I_k and * represents the complex conjugate.

For a deuterium-to-metal (D/M) concentration, x, the average residence time $\tau(x)$ of a given deuterium atom is given by

$$\tau(x) = \tau_0/V(x) \tag{4}$$

and we define an effective residence time, τ_{eff}, such that

$$\tau_{\mathrm{eff}} = \tau(x)/f_t(x) \tag{5}$$

where f_t is the tracer correlation factor, V is the effective vacancy concentration (or

target site availability factor) and τ_0 is the residence time in the low-concentration limit at the same temperature. f_t describes the enhanced probability of a return jump over forward jumps at finite concentration, given that site blocking exists. In general f_t will be a function of time in that the first jump in an examined sequence is uncorrelated, whereas the second and subsequent jumps *are* correlated. Thus as $\omega \to \infty$, $f_t \to 1$ and as $\omega \to 0$, $f_t \to f_t(\infty) < 1$ and the lineshape is no longer precisely Lorentzian in energy transfer (Ross and Wilson 1978, Faux and Ross 1987b). In the present investigation, the time and Q-dependence of the correlation factor are not introduced explicitly and so τ_{eff} incorporates the average correlation effect. For simple site blocking (no double occupancy), V is simply equal to the vacancy concentration $(1 - \frac{1}{8}x)$. However, for more extensive site exclusion, this is no longer true. Monte-Carlo calculations of $V(x)$ for no double occupancy, and blocking to the first, second and third nearest interstitial neighbours for the BCC tetrahedral lattice have been performed (Faux and Ross 1987a), but the case for a real (soft) potential has not been worked out.

In a recent publication (Sinha and Ross 1988), a formalism has been developed for the coherent scattering function of a collection of diffusing interstitials which mutually interact. This has been done on the basis of a mean-field calculation of the particle density response function. This is analogous to the random-phase approximation (RPA) treatment of the system of interacting electrons examined by Hayashi and Shimizu (1969), where

$$S(\boldsymbol{Q}, \omega) = \frac{1}{\pi} \frac{1}{e^{\hbar\omega/kT} - 1} \operatorname{Im}\{\chi(\boldsymbol{Q}, \omega)\} \tag{6}$$

and the zero interaction response function is given by

$$\chi_0(\boldsymbol{Q}, \omega) = \frac{x(1-x)}{kT} \frac{1}{1 - i\omega\Gamma(\boldsymbol{Q})^{-1}}. \tag{7}$$

If equation (7) is applied to the Rowe *et al* formalism we are left with an expression in matrix form for χ_0 given by

$$\chi_0^{kk'}(\boldsymbol{Q}, \omega) = \frac{x(1-x)}{kT} [1 - i\omega\Gamma_{kk'}(\boldsymbol{Q})^{-1}]^{-1} \tag{8}$$

where $\Gamma_{kk'}(\boldsymbol{Q}, \omega)$ is an element of the broadening matrix $\mathbf{A}$ in equation (1) and '-1' now implies the inverse of the matrix. Mutual interactions are introduced into the response function via the appropriate potential matrix linking nearest-neighbour sites k and k', so that, ignoring phonon coupling, the response function becomes

$$\chi^{kk'}(\boldsymbol{Q}, \omega) = \chi_0^{kk'}(\boldsymbol{Q}, \omega)/[1 + V_{kk'}(\boldsymbol{Q})\chi_0^{kk'}(\boldsymbol{Q}, \omega)] \tag{9}$$

where $V_{kk'}(\boldsymbol{Q})$ is the Fourier transform of $V_{kk'}(\boldsymbol{r})$. The coherent scattering function, $S_{\text{coh}}(\boldsymbol{Q}, \omega)$, can then also be expressed as a sum of six Lorentzians, where the widths of each component are 'narrowed' by a partial structure factor, $S^{kk'}(\boldsymbol{Q})$. That is, the coherent line width is proportional to the incoherent line width, divided by $S^{kk'}(\boldsymbol{Q})$ which is related to $V_{kk'}(\boldsymbol{Q})$ by

$$S^{kk'}(\boldsymbol{Q}) = x(1-x)\, e^{-2W}/(1 + x(1-x)V^{kk'}(\boldsymbol{Q})/kT). \tag{10}$$

For spherical symmetry $S^{kk'}(\boldsymbol{Q})$ becomes $S(Q)$, the total structure factor, and it is in this approximation that the coherent scattering function has been fitted. The coherent scattering function may then be expressed (in a non-factorised form for clarity), as

$$S_{\text{coh}}(Q, \omega) = \frac{S(Q)}{\pi} \sum_{j=1}^{6} \frac{W_j x(1-x)\lambda_j / S(Q)\tau_0^{\text{eff}}}{(x(1-x)\lambda_j / S(Q)\tau_0^{\text{eff}})^2 + \omega^2} e^{-2W}. \tag{11}$$

where, in analogy with the incoherent case, τ_0^{eff} incorporates the average mobility

correlation effect, i.e.

$$\tau_0^{\text{eff}} = \tau_0 / f_{\text{m}} \tag{12}$$

where f_{m} is the mobility correlation factor.

In the low-Q limit, both the incoherent and coherent scattering laws reduce to single Lorentzians which intrinsically describe the long spatial and time ranges of the motion. In these limits the correlation factors have therefore approached their asymptotic values for $t \rightarrow \infty$ and the macroscopic averaged behaviour is observed. The scattering functions in (2) and (11), at low Q, then become

$$S_{\text{inc}}(Q, \omega) = \frac{1}{\pi} \frac{D_{\text{t}} Q^2}{(D_{\text{t}} Q^2)^2 + \omega^2} \, \text{e}^{-2W} \tag{13}$$

$$S_{\text{coh}}(Q, \omega) = \frac{S(Q)}{\pi} \frac{D_{\text{c}} Q^2}{(D_{\text{c}} Q^2)^2 + \omega^2} \, \text{e}^{-2W} \tag{14}$$

where D_{t} and D_{c} are the tracer and chemical diffusion coefficients respectively. D_{t} gives the macroscopic diffusion rate of the individual particle and D_{c} gives the corresponding relaxation rate of density fluctuations which are caused by interparticle interactions. These diffusion coefficients can be expressed in terms of the correlation factors, f, and the site availability, V, as follows:

$$D_{\text{t}} = f_{\text{t}} V D_0 \tag{15}$$

$$D_{\text{c}} = f_{\text{m}} V \gamma D_0 \tag{16}$$

where D_0 is the diffusion coefficient approximate to zero interstitial concentration and $\gamma(Q \rightarrow 0)$ is the thermodynamic factor which, for a system exhibiting only concentration–concentration fluctuations, is also the reciprocal of $S(0)$, the structure factor at zero wave vector transfer. (The influence of elastic stresses is discussed later in this paper.) The ratio of D_{c} to D_{t} is then given as

$$D_{\text{c}} / D_{\text{t}} = (f_{\text{m}} / f_{\text{t}}) \gamma(0) = \gamma(0) / H_{\text{R}} \tag{17}$$

where H_{R} is commonly referred to as Haven's ratio.

3. Experimental details and measurements

In order to apply these ideas, we used the diffuse scattering spectrometer D7 at the Institut Laue–Langevin, Grenoble, in the configuration for polarisation analysis with time-of-flight (TOF) energy analysis. The TOF pulse was produced by a four-slit disc chopper at 9000 rpm. This had advantages over the pseudostatistical chopper option in that it gave a much smaller background, thus enabling the scattering in the wings of the quasielastic peak to be determined with greater accuracy. An energy resolution ranging between 96 and 115 μeV over the detector bank, together with a TOF channel width of 19 μs, were found to be suitable to resolve well the line broadenings expected at 600 K. The incident neutron energy of 3.52 meV was selected using a graphite monochromator. The monochromatic beam was then polarised using a supermirror polariser before passing through a 'flipper', a coil device which flips the neutron spin when switched on and leaves it in its original spin state if switched off. Beyond the flipper, the beam was

passed through the disc chopper and then through a slit system situated in front of the sample table to define the beam width on the sample. The scattered neutrons were then detected in ^{3}He counters, arranged in four banks, each of variable angle. For the spin analysis, supermirror analysers (similar to the polariser), were positioned in front of the detectors and adjusted for angle in the horizontal plane for maximum transmission. Details of the general properties and performance of these supermirror polarising elements can be found in Schärpf (1989a, b). The analysers were arranged so as to accept only those neutrons which had the same spin direction as those in the incident beam. In other words, in the ideal case, only the non-spin-flipped scattered neutrons would be detected with the flipper off and with the flipper on, only the neutrons which had undergone a spin flip would be detected. The instrument ran alternately with flipper on and off and with an interval determined by a preset incident monitor count until the required number of counts was achieved.

In the present investigation, we have used deuterium to an interstitial concentration of 70% D:M in a single crystal of niobium, which, after removal of the surface oxide layer, was palladium coated in order to catalyse the deuterium chemisorption at the surface. The crystal was cylindrical and of approximately 14 mm diameter which, at this concentration, gave a predicted 17% scattering for a uniform incident neutron flux normal to the crystal axis. The container was made of a high melting point aluminium alloy, having a wall thickness of about 0.5 mm and a bore just large enough to accept the crystal (allowing for its lattice expansion when loaded with deuterium). In this way the scattering from the gas outside of the crystal could be minimised. The sample can itself was passed between the windings of furnace. The deuterium loading was done *in situ* in order to ensure that the deuterium-loaded sample remained at a temperature above its α–β phase transition. This avoided the inevitable generation of dislocation networks in the crystal which occurs subsequent to such phase changes. The unloaded crystal was therefore raised to 600 K (well into the single α-phase region) under a high vacuum before the sample was exposed to any deuterium pressure. At this temperature and for 70% deuterium, the equilibrium pressure is around 0.1 bar. However, because of the slow deuterium uptake, the crystal was initially exposed to about 2 bar deuterium pressure (within the yield limits of the can) and for a controlled period to speed up the rate of chemisorption. In addition to using volumetric calculations, the quantitative uptake of the crystal was monitored by measuring the sample transmission as a function of time. The high deuterium concentration provided the large Q-dependent variation in structure factor, $S(Q)$, which is required to make the theoretically predicted narrowing behaviour of the coherent quasielastic line sufficiently pronounced. Figure 1 shows the Ewald construction for the locus of the elastic scattering. This locus was chosen to approach the superlattice peak at [2, 1, 1] where the structure factor, and therefore the narrowing of the coherent peak, might be expected to be maximised.

Before performing any sample scattering runs, the flipping ratio, R, was measured using a fused quartz sample (see Schärpf 1985) which scatters very diffusely and without spin flip. The flipping ratio is a measure of the efficiency of the whole system with respect to propagation of the correct neutron spin and it is affected by the polarising efficiency of the polariser and analyser, the flipper efficiency and the depolarisation of the beam in the intervening sections. The depolarisation was minimised by the use of guide fields in the incident and scattered beams and the avoidance of magnetic materials in the sample environment. R is measured simply as the ratio of the detected intensity from the non-flipping sample with the flipper off to that with the flipper on and, ideally, this should be infinite. For this experiment, R was about 16. That is, we could expect that, on average, 1 in 16 neutrons would be transmitted through the system with the wrong spin.

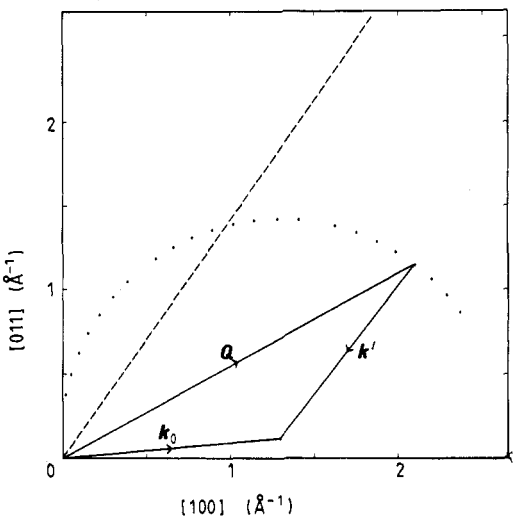

Figure 1. The locus of detectors (dots) in the reciprocal scattering plane for elastically scattered neutrons.

Using an incident wavelength of 4.82 Å and a Be filter to reduce the $\lambda/2$ and higher-order monochromator reflections, the scattering runs may be summarised as follows:

Quartz	(↑ ↑, ↑ ↓)
Vanadium spiral	(T)
Empty can	(T)
Cd	(T, ↑ ↑, ↑ ↓)
Nb	(T, ↑ ↑, ↑ ↓)
$NbD_{0.7}$	(T, ↑ ↑, ↑ ↓)

where ↑ ↓ and ↑ ↑ are the scattering cases with the flipper on and off respectively and with polarisation analysers in front of the detectors and T (total) denotes the case where the analysers were removed and thus no distinction between the scattered spin state was made. The Nb, Cd and empty can runs were necessary for the sample and vanadium background corrections and the quartz run, which was also corrected for background, was made in order to determine the flipping ratio, as mentioned previously.

4. Data correction and analysis

The data reduction was performed on the time-of-flight data and a brief summary is given here. A fuller account of data treatment for polarisation analysis experiments, with particular reference to the D7 instrument, is given by Schärpf (1985). For brevity, we use the symbol I to denote intensities normalised to the incident beam monitor (M1). If a correction is repeated for the cases ↑ ↑, ↑ ↓, and T, the general superscript α will be used. Monitor 2 (the beam stop monitor) is denoted by M2. The background corrections were calculated from the Nb and Cd runs using the following approximation:

$$I^{\alpha}_{\mathrm{bkd}} \simeq \mathrm{Y}^{\mathrm{D}} I^{\alpha}_{\mathrm{Nb}} + (1 - \mathrm{Y}^{\mathrm{D}}) \cdot I^{\alpha}_{\mathrm{Cd}}$$

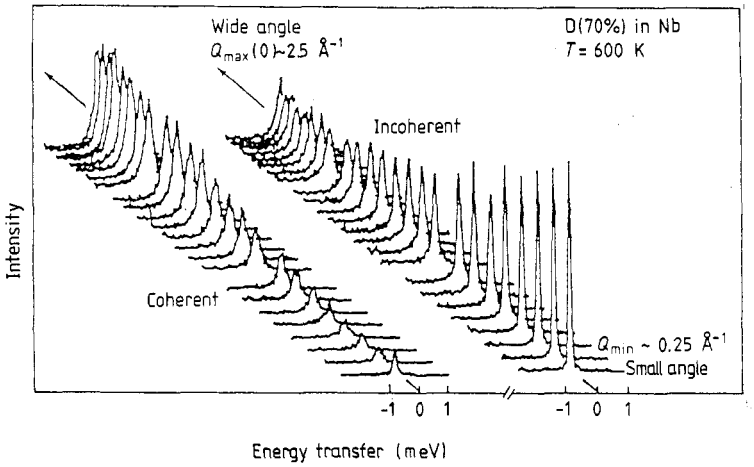

Figure 2. The separated coherent and incoherent parts of the total scattering around the elastic position as a function of detector angle.

where Y^D is the sample transmission factor, measured as,

$$Y^D \simeq (I^{M2}_{NbD} - I^{M2}_{Cd})/(I^{M2}_{Nb} - I^{M2}_{Cd}).$$

The deuterium scattering was then obtained as,

$$I^{\alpha}_D = I^{\alpha}_{NbD} - I^{\alpha}_{bkd}.$$

The $I_D^{\uparrow\downarrow}$ and $I_D^{\uparrow\uparrow}$ intensities were then corrected for flipping ratio by subtracting $1/R$ of the opposite spin component from each. From these corrected intensities, the analyser transmission as a function of energy transfer was determined by comparing the sum of the $I_D^{\uparrow\downarrow}$ and the $I_D^{\uparrow\uparrow}$ intensities with the I^T_D intensity, the difference being due to the analyser transmission factor, $Y^A(\omega)$, i.e.

$$I_D^{\uparrow\downarrow}(\omega) + I_D^{\uparrow\uparrow}(\omega) = Y^A(\omega)T^T_D(\omega).$$

The vanadium run was corrected for background in an analogous way,

$$I^{corr}_V \simeq I^T_V - (1 - Y^V)I^T_{Cd} - Y^V I^T_{empty}$$

where Y^V is given by,

$$Y^V \simeq (I^{M2}_V - I^{M2}_{Cd})/(I^{M2}_{empty} - I^{M2}_{Cd}).$$

Finally the $I_D^{\uparrow\downarrow}$ and $I_D^{\uparrow\uparrow}$ intensities were corrected for analyser transmission and normalised to the vanadium result which, of course, required no analyser transmission correction. The separated incoherent and coherent components of the scattering are shown in figure 2.

The multiple-scattering correction was performed using a version of the Harwell Monte-Carlo program DISCUS (Johnson 1974), which was modified to calculate, separately, the corrections for the $\uparrow\downarrow$ and $\uparrow\uparrow$ scatterings. This required input of both the coherent and incoherent scattering functions which were in fact calculated in separate subroutines. Since multiply-scattered neutrons can have passed through a variety of points in reciprocal space and energy transfer, the following procedure was adopted to approximate the scattering functions over a wide range of Q and ω: the initial incoherent spectra were fitted individually to obtain good approximations to the quasielastic half

widths, Γ_{inc}. These spectra were then fitted simultaneously to the six-component Lorentzian model of equation (2), where the effective residence time, τ_{eff}, was one of the refined parameters. The individual broadenings, Γ, were finally fitted to the following model in Q using the value of τ_{eff} from the simultaneous fit:

$$\Gamma(Q) = \hbar/\tau_{eff}(1 - \sin(Ql)/(Ql)). \tag{18}$$

The fit was made by refining only an amplitude factor. The nearest-neighbour jump distance, l, was kept constant on the grounds that it was well known. This treatment of the half widths is equivalent to a liquid or polycrystalline approximation, thus giving a kind of spatial average. For the coherent scattering, a simultaneous fit of the six-Lorentzian model of equation (11) was made in order to determine the $S(Q)$ values and, for the purposes of the multiple-scattering program, the coherent scattering function widths were calculated as

$$\Gamma_{coh}(Q) = \Gamma_{inc}(Q)/S(Q).$$

The $S(Q)$s used in the calculation of the total scattering cross section, σ_s, within the DISCUS program were, however, determined using the values of the Cowley short-range order parameters obtained by Hempelmann *et al* (1988) for a deuterium concentration of 0.72 and $T = 581$ K in a polycrystalline niobium sample. This was done in order to make the following simplifying approximation:

$$\frac{1}{4\pi}\int S(Q)\,\mathrm{d}\Omega \simeq S^{P}(Q)$$

where $S^{P}(Q)$ is the polycrystalline $S(Q)$.

The $\uparrow\downarrow$ and $\uparrow\uparrow$ data were corrected to fourth-order scattering and three self-consistent iterations of the above process resulted in a satisfactory convergence of the correction factors.

The vanadium data were found to be well fitted by a Gaussian in energy for each detector and the resolution function was calculated from the fit parameters. The centres were defined as zero for each. The corrected incoherent spectra were fitted both individually and simultaneously, however, those spectra having a line broadening of less than 10% of the resolution width were excluded from the fits. This was because of the risk of introducing a large numerical uncertainty in the line broadenings extracted from fits where there was a gross mismatch between the quasielastic broadening and the width of the resolution function. This error arises in the function convolution stage. The simultaneous fits enabled the tying together of parameters expected to be common to each spectrum, thus constraining the fitting process much more strictly than for the individual fits. The variable parameters used for fitting to the incoherent data were: a flat background, a sloping background (which was linear in energy transfer), a Q^2-dependent inelastic background (for simultaneous spectrum fits), an overall intensity factor, an effective residence time and a peak centre position in energy transfer. The peak centres were determined from the individual spectrum fits. These positions were then used as non-variable input for the simultaneous fit and acted as spectrum centre shifts, while a common centre position was refined. A similar procedure was adopted for the fitting of the coherent data but this time the line widths were narrowed by the values of $S(Q)$ and the residence time parameter was τ_0. It was necessary, for some spectra, to exclude certain areas in ω where there were evidently overlapping inelastic features and some spectra were omitted completely. In view of the high degree of covariance between the intensity and the line width, combined with the low statistics of the coherent scattering at low Q, the following 'smoothing' function was fitted to the

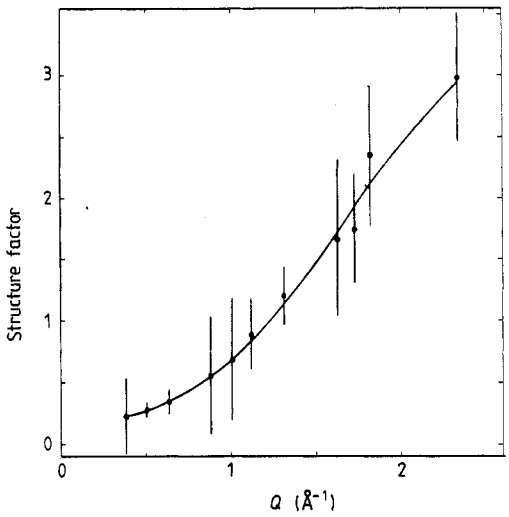

Figure 3. The coherent structure factor as a function of Q. The discrete points are the values derived from the individual spectrum fits and the curve represents the values of the best fit of expression (19) to these values multiplied by the common refinement parameter which gave an optimal simultaneous spectrum fit of these smoothed $S(Q)$ values.

individually fitted $S(Q)$ values:

$$S(Q) = (1 - c) \sum_i Z_i \alpha_i \frac{\sin(Qr_i)}{Qr_i} \tag{19}$$

where $c = \frac{1}{8}x$, the deuterium concentration in units of atoms per interstitial site, r_i is the distance to the ith nearest-neighbour site and Z_i is the coordination number. This is equivalent to the polycrystalline expression for $S(Q)$ using the Cowley short-range-order formalism. However, the parameters α_i here cannot have any simple physical significance attached to them as for the polycrystalline case. For this fit, a sum over the first four terms ($i = 0$ to 3), was found to be sufficient to provide a good overall description of the $S(Q)$ data and two approaches were adopted in order to identify systematic errors arising from this process. Firstly, expression (19) was fitted to the values of $S(Q)$ obtained from the individual coherent spectrum fits. The resulting values of the fitted function at each Q were introduced as values of $S(Q)$ in the simultaneous spectrum fit and refined by a common multiplying parameter. Figure 3 shows both the values of $S(Q)$ from the individual spectrum fits together with the refined function values from the simultaneous fit (points on the curve). Secondly, $S(Q)$ was calculated according to (19) in the spectrum fit itself and α_1–α_3 were refined. The refined values of $S(Q)$ obtained from the former method were re-introduced as fixed parameters into the individual spectrum fits in order to determine the final values of the residence times for the individual coherent spectra. In all cases, the errors on the parameters were calculated from their gradients around their fit values. We note that $S(Q)$ changes by more than an order of magnitude in the measured scattering, thus providing a good test of equation (11).

5. Results

Figure 2 shows the separated incoherent and coherent scattering around the elastic position which exhibit the expected qualitative features: the incoherent peak narrows as $Q \rightarrow 0$ and the diffuse coherent quasielastic peak is low in intensity and broad at low

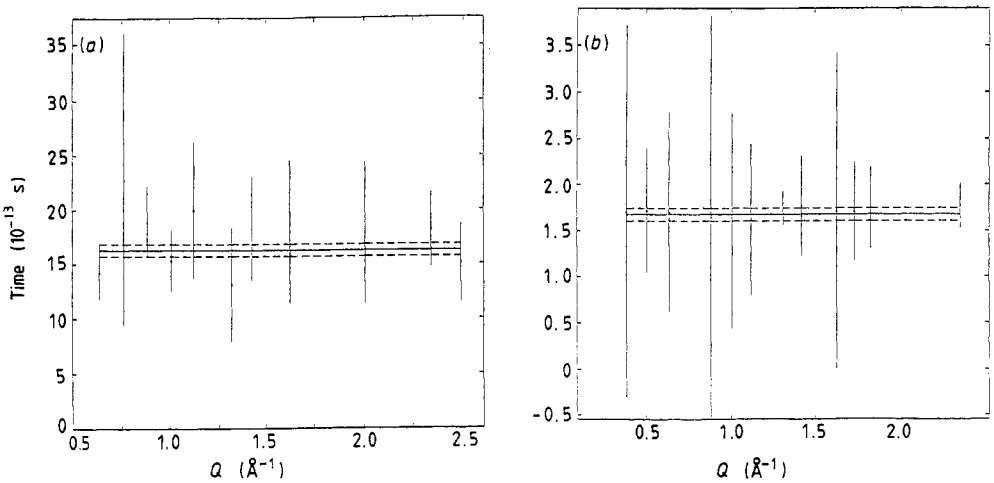

Figure 4. The individually and simultaneously fitted residence times from: (*a*), the incoherent scattering; (*b*), the coherent scattering. (The broken lines indicate the error level of the simultaneous fits.)

Q and peaks in intensity around the superlattice peak position where a narrowing process is in evidence.

Figure 4 shows the individually and simultaneously fitted τ-values for the incoherent and coherent scattering where the errors in the simultaneous fit parameters are represented by the broken lines. For the incoherent case τ_{eff} is the plotted parameter, and for the coherent case the parameter is τ_0. The horizontal straight lines represent the simultaneously fitted τ-values. Figure 5 shows the corrected incoherent and coherent

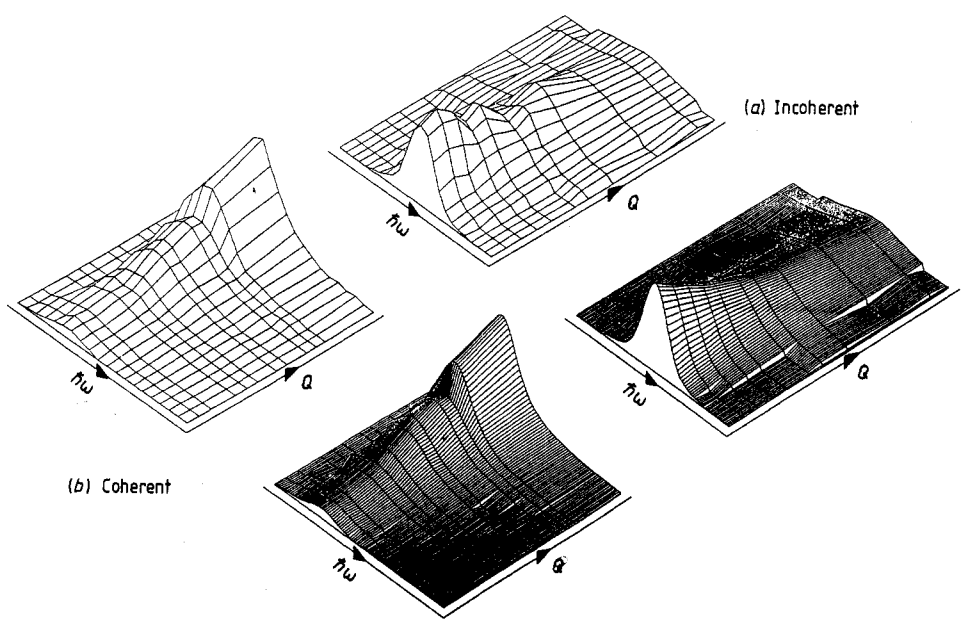

Figure 5. The corrected data in Q and ω (left) and the corresponding simultaneous fit (right) for the incoherent and the coherent spectra.

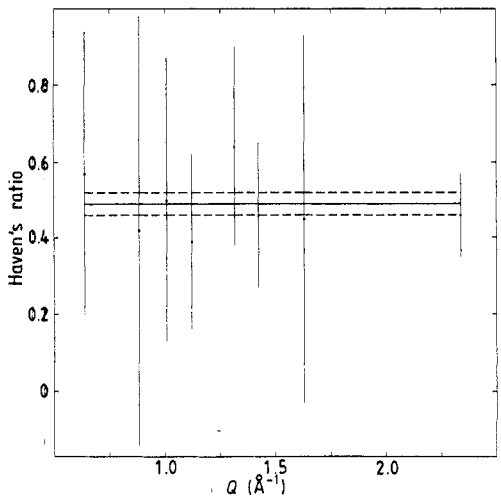

Figure 6. Haven's ratio determined from the individual and simultaneous spectrum fits as a function of Q. (The broken lines indicate the error estimate derived from the simultaneously fitted parameters.)

data (interpolated onto a common grid in energy) with their corresponding spectrum fits. Truncations in these plots are due either to the termination of a particular data set or where an inelastic feature has been excluded. In these regions, the intensity is set to zero. The data and the corresponding fit are shown on the same vertical and horizontal scales for ease of comparison.

By comparing equations (2) and (11) with (13) and (14) and using equation (17), we may deduce that, in the present formalism,

$$[x(1-x)\tau_{\text{eff}}]/S(Q)\tau_0^{\text{eff}} = \gamma(Q)/H_{\text{R}} \tag{20}$$

and inserting $\gamma(Q) = 1/S(Q)$, this gives Haven's ratio as

$$H_{\text{R}} = \tau_0^{\text{eff}}/(x(1-x)\tau_{\text{eff}}). \tag{21}$$

This also implies that the effective coherent residence time, $\tau_{\text{coh}} = \tau_0/x(1-x)$, is simply related to the effective incoherent residence time by

$$\tau_{\text{coh}} = H_{\text{R}}\tau_{\text{inc}}. \tag{22}$$

Figure 6 shows the values of H_{R} calculated from expression (22) using the individually and simultaneously fitted residence times for the incoherent and coherent dynamics. The horizontal straight line is the value of 0.49 ± 0.03, obtained by using the simultaneously fitted residence times, and this is in agreement with the average of the value of H_{R}, $\langle H_{\text{R}} \rangle = 0.49 \pm 0.08$, given by inserting the individually fitted residence times. Again the broken lines represent the error level derived from the errors of the simultaneous fit parameters.

The two methods employed for fitting $S(Q)$ did indeed show a systematic error in determining a reliable value for $\gamma(0)$ $(=1/S(0))$ giving $\gamma(0) = 5.9$ and 7.0 in the two cases. We can therefore expect the systematic error in the value of the thermodynamic factor to be at least of the order of 20%.

Now, if D_{t} is calculated as

$$D_{\text{t}} = f_{\text{t}}l^2/6\tau(x) = l^2/6\tau_{\text{eff}} = a^2/48\tau_{\text{eff}} \tag{23}$$

we arrive at a value for the tracer diffusion coefficient of $(1.49 \pm 0.05) \times 10^{-5}\ \text{cm}^2\ \text{s}^{-1}$. This compares with a value of $(1.21 \pm 0.09) \times 10^{-5}\ \text{cm}^2\ \text{s}^{-1}$ obtained by fitting equation (13) to the low-Q spectra ($Q < 0.9\ \text{Å}^{-1}$). Now using equation (17) and the value for H_{R},

and taking the mean value of $\gamma(0)$ of 6.45, we predict a chemical diffusion coefficient, D_c, of $(1.96 \pm 0.44) \times 10^{-4}$ cm^2 s^{-1}. Fitting expression (14) to the coherent data in the low-Q approximation with a common $S(Q)$ intensity factor gave $D_c = (1.0 \pm 0.4) \times 10^{-4}$ cm^2 s^{-1}, a quite different value, and a characteristic $S(Q)$ of 0.21 ± 0.03, close to $x(1-x)$, the Laue intensity. It must be noted, however, that the statistics at low Q in the coherent scattering are relatively poor. Also the constant-intensity assumption is not completely valid for the present data since $S(Q)$, even at the lowest Q-values, shows evidence of structure.

6. Discussion

A study of the fitted residence times shown in figure 4 seems, within the accuracy of the present experiment, to show little convincing evidence of any Q-dependence. The constant-τ model used for the present analysis is therefore a reasonable approximation, even given that there is a possible ω-dependence of τ. Hitherto unpublished Monte-Carlo calculations (Faux 1986) showing the time dependence of f_t for the case of simple site blocking (no double occupancy) in a simulation of the presently studied system, show that most of the change in the value of f_t takes place over about four or five attempted jumps per interstitial. This corresponds to an ω range of, say, $1/5\tau_0$ to ∞. However, the site blocking is expected to extend to several nearest-neighbour distances and we might expect that the real time for the interstitial to make a series of correlated hops becomes longer. This means that the lineshape should still be changing in a significant way even closer to the peak centre than for the simple blocking system. If we then examine the quasielastic peak out to about 5 HWHM in energy transfer ($\sim 5/\tau_0$), we are covering a time range in which the change in value of the correlation factor is expected to be important. It must be concluded, therefore, that the statistics of the present data at the current energy resolution are not sufficient to identify, with any certainty, a deviation of the lineshape from a Lorentzian in energy due to time-dependent correlations. This might also indicate that the Q-dependence of this time dependence is small, since the data is adequately described over the whole Q-range by a single residence time parameter. The relatively large errors that occur, particularly for the individually fitted incoherent and coherent residence times (and hence for Haven's ratio), are a reflection on the statistics of the data combined with a comparatively small number of degrees of freedom for some of the individual fits. For the coherent data in particular, the minimum for some of the parameters was rather flat. By fixing $S(Q)$ and the background at the simultaneous fit values in the individual fits, some degree of 'fixing' was thereby imposed on the residence time parameter. This is because $S(Q)$ and τ, although not having precisely the same functional behaviour in the coherent scattering function, have nonetheless a large covariance. This meant that the individually fitted τ-values had a tendency to stay close to the simultaneous fit value and that the spread of these values was more characteristic of the error on the simultaneous fit. The restriction on τ due to the fixing of $S(Q)$ has therefore had the effect of giving a statistical spread of the coherent residence times somewhat smaller than the size of the error bars and this is also reflected in the values of Haven's ratio that were calculated from them.

The value obtained for the tracer diffusion coefficient of $(1.49 \pm 0.05) \times 10^{-5}$ cm^2 s^{-1} is comparable with, but greater than, what we would expect from an extrapolation, in T and x, of the results obtained by Hempelmann *et al* (1988) which gives a value around 1.1×10^{-5} cm^2 s^{-1} for $x = 0.7$ and $T = 600$ K. However, the chemical diffusion coefficient obtained in the present analyisis of $(1.96 \pm 0.44) \times 10^{-4}$ cm^2 s^{-1} is much

larger, the corresponding extrapolation here giving an estimated value of D_c of around 7.0×10^{-5} cm^2 s^{-1}. This discrepancy might be attributed, in part, to a systematic error which can occur in the fitting process whereby variable parameters such as $S(Q)$ and τ have a certain freedom to exchange value if the systematic error thus introduced is comparable with, or less than, the statistical error of the data. That is, equivalently good fits in χ^2 can be achieved for a *range* of $S(Q)$ values and the corresponding τ-values. However, this difference could also be due to a change of the physical processes contributing to the particle density response with changes in Q. This could be readily verified if reliable values of $S(Q)$ were available from a fit-independent method such as spectrum integration, for example, where a possible Q-dependence of the residence time could be realistically investigated. The value of D_c extrapolated from the data of Hempelmann *et al* is, in fact, much closer to the value of $(1.0 \pm 0.4) \times 10^{-4}$ cm^2 s^{-1} obtained in the present investigation from the spectrum fit at low Q, and therefore we can say that the present experiment agrees quite well at low Q, where their measurements were confined.

The present neutron scattering results show, once again, a significant discrepancy in the values of the chemical diffusion coefficient with respect to those obtained from Gorsky effect measurements (the neutron results giving consistently higher values). This difference is only important where spinodal decomposition to the α'-phase and the formation of a superlattice can occur. At higher concentrations ($x \sim 1$), however, β-phase precipitation is preferred because the effective hard-sphere potentials touch. In this case, clustering is no longer important and coherency stresses do not appear. In a recent communication by Wipf *et al* (1989), it has been demonstrated numerically, using a theory due to Wagner and Horner (1974) and Wagner (1978), that the discrepancy in the neutron scattering and Gorsky effect data for $x \sim 0.5$ can indeed be explained in terms of coherency stresses. Coherency stresses have the effect of increasing the elastic energy over the comparatively short spatial ranges, measured by most neutron scattering experiments, where the short-wavelength 'bulk-mode' density fluctuations are concentrated. In Gorsky effect measurements, on the other hand, the lower energy 'macroscopic' modes (which have wavelengths comparable with the size of the crystal) are probed and on these length scales the coherency stresses are much lower or even zero. They therefore propose that the neutron studies, which are sensitive to the shorter wavelength modes, measure a fundamentally different diffusion coefficient and thermodynamic factor which they term D_{bulk} and f_{bulk}, respectively. Using their notation these may be written as

$$D_{\text{bulk}} = D_{\text{chem}}[1 + \rho(E_1 - E_{\text{bulk}})/k_B T f_{\text{therm}}]$$

and

$$f_{\text{bulk}} = f_{\text{therm}}[1 + \rho(E_1 - E_{\text{bulk}})/k_B T f_{\text{therm}}]$$

where E_1 is the energy of the macroscopic mode, E_{bulk} is the energy of the bulk mode and D_{chem} and f_{therm} represent the 'true' values of the chemical diffusion coefficient and thermodynamic factor, respectively, obtained from Gorsky effect measurements. It has been shown by Wipf *et al* that the introduction of the right-hand term in the above expressions for the neutron data analysis does indeed account for the difference between the existing Gorsky effect data and the specific results of Hempelmann *et al*. However, we might well expect this term to be Q-dependent, since the bulk mode energy spectrum should change on different length scales. It might therefore be expected that as Q is increased, the neutron results would increasingly diverge from the Gorsky effect data as the higher energy bulk modes are probed and that as $Q \rightarrow 0$, they could converge to

the same value. This is a point which is not mentioned by Wipf *et al*, although most of the Q-dependence will probably occur over spatial distances not much smaller than the size of the crystal, since the stress relaxation lies in the ability of the free boundaries to distort. Comparison of the present neutron experiment with that of Hempelmann *et al* does seem to indicate a process of this kind, in that the fits characterised by higher Q-values give a generally increased chemical diffusion coefficient. This favours the proposal that the discrepancy in the results of the neutron experiments could be attributed to a Q-dependent change of physical processes in the particle density response.

The values of the thermodynamic factor for both experiments are very similar. However, a large discrepancy lies in the value for H_R which Hempelmann *et al* have reported to be 0.98 for $x = 0.72$ and $T = 581$ K. This, taken by itself, would give a corresponding discrepancy in the value of the chemical diffusion coefficient for the two experiments by nearly a factor of two if derived from expression (17) for the same tracer diffusion coefficient. Now, if we use the Monte Carlo calculations of f_t and f_m performed by Faux and Ross (1987a) we predict the following values of H_R for the second and third nearest-neighbour 'hard-sphere' tetrahedral site blocking and for $x = 0.7$

$$H_R = 0.857$$

$$H_R = 0.613.$$

Here our value of around 0.49 would indicate a highly correlated motion with a blocking radius greater than that of the third nearest neighbour. However, if the value of the thermodynamic factor measured is in fact f_{bulk}, then the values of H_R obtained from equation (20), for example, would tend to be underestimated. One possible solution to this problem could be to introduce a bulk mode potential into the response function in expression (9).

Using equations (4), (5) and (12), we can relate τ_0^{eff} and τ_{eff} and we have

$$\tau_0^{eff} = (f_t/f_m)V\tau_{eff} = H_R V\tau_{eff}.$$

If we now use the values of V from the Monte-Carlo calculations of Faux and Ross mentioned above, we predict the following values of τ_0^{eff} for the two site blocking cases

$$\tau_0^{eff(2)} = 8.53 \times 10^{-13} \text{ s}$$

$$\tau_0^{eff(3)} = 1.94 \times 10^{-13} \text{ s}.$$

The value of τ_0^{eff} derived from the present coherent fit ($\tau_0^{eff} = (1.68 \pm 0.07) \times 10^{-13}$ s) lies outside these limits and indicates an effective site blocking radius extending beyond the third nearest neighbour. This is in general agreement with the extent of blocking predicted from the measured values of Haven's ratio.

The magnitude of the correlation effect that we are seeing in this experiment is perhaps not totally surprising since the maximum theoretical concentration for a random distribution of interstitials on the tetrahedral symmetry lattice, with third nearest-neighbour site blocking is around $x = 0.8$ and so the effective vacancy concentration is quite small. In all, even using this rather simplistic hard-sphere potential, we would conclude that, at a concentration of $x = 0.7$, we are seeing a characteristic site blocking of greater than, but in the region of, three nearest-neighbour shells (that is $\geqslant 2.1$ Å in the expanded niobium lattice). This is therefore not in disagreement with the value of 2.1 Å proposed by Westlake (1980) as the minimum separation of hydrogen in metals based on electron band calculations.

In conclusion, we have succeeded in separating, experimentally, the two components

of the quasielastic scattering of a high concentration deuterium lattice gas in niobium to a high wave vector transfer. We have shown that the approximations of neglecting time-dependent correlations and vector interactions has not markedly hindered the explanation of the data, in terms of simplified models, over a remarkably wide range in Q. We would note that this is, to the best of our knowledge, the first report of the use of polarisation analysis to separate the tracer and collective diffusion properties of a quasielastic scattering sample. With improved neutron sources and the optimisation of the instrumentation, it is likely that this technique will become more important in the future.

References

Chudley C T and Elliott R J 1961 *Proc. Phys. Soc.* **77** 353
Faux D A 1986 *PhD Thesis* Birmingham University, UK
Faux D A and Ross D K 1987a *J. Phys. C: Solid State Phys.* **20** 1441
—— 1987b *J. Less-Comm. Met.* **129** 229
Hayashi E and Shimizu M 1969 *J. Phys. Soc. Japan* **26** 1396
Hempelmann R, Richter D, Faux D A and Ross D K 1988 *Z. Phys. Chem., NF* **159** 175
Johnson M W 1974 *AERE Report* R-7682
Ross D K and Wilson D L T 1978 *Neutron Inelastic Scattering, 1977* vol 2 (Vienna: IAEA) p 383
Rowe J M, Sköld K, Flotow H E and Rush J J 1971 *J. Phys. Chem. Solids* **32** 41
Schärpf O 1985 *Neutron Scattering in the 'Nineties (IAEA Proc. Ser.)* (Vienna: IAEA) p 85
—— 1989a *Physica* B **156/157** 631
—— 1989b *Physica* B **156/157** 639
Sinha S K and Ross D K 1988 *Physica* B **149** 51
Wagner H 1978 *Hydrogen in Metals I: Topics in Applied Physics* vol 28, ed G Alefeld and J Völkl (Berlin: Springer) p 5
Wagner H and Horner H 1974 *Adv. Phys.* **23** 587
Westlake D G 1980 *J. Less-Common. Met.* **75** 73
Wipf H, Völkl J and Alefeld G 1989 *Z. Phys.* B **76** 353